MD simulation of epitaxial recrystallization and defect structure of Al-implanted 4H-SiC

Sabine Leroch[1]*, Robert Stella[1], Andreas Hössinger[2], and Lado Filipovic[1]
[1]CDL for Multi-Scale Process Modeling of Semiconductor Devices and Sensors, at the Institute for Microelectronics, TU Wien, 1040 Vienna, Austria
[2]Silvaco Europe Ltd., St Ives, Cambridgeshire, PE27 5JL, United Kingdom
*Email: leroch@iue.tuwien.ac.at

2024 International Conference on Simulation of Semiconductor Processes and Devices (SISPAD) | 979-8-3315-1635-2/24/$31.00 ©2024 IEEE | DOI: 10.1109/SISPAD62626.2024.10733052

***Abstract*—We have performed a molecular dynamics study for the recrystallization of Al-implanted 4H-SiC in dependence of annealing temperature and time. We show in that the principal physical picture of recrystallization is in line with experiments and former MD simulations with respect to the activation energy of recrystallization and its onset temperature (the minimum temperature necessary to initiate full recyrstallization of amorphous SiC). The annealed structures are poly-crystalline and show point defects, defect complexes, but also extended defects like interstitial clusters and stacking faults in dependence of the annealing temperature. Most of the residual defects are thermally stable and need longer annealing times than those accessible with MD simulations alone.**

***Index Terms*—Al-implantated 4H-SiC, activation energy for recrystallization, expitaxial regrowth, point defects, defect complexes and clusters**

I. Introduction

The 4H-SiC structure is highly technologically relevant and provides the widest band gap (3.26 eV) from the available SiC polytypes. Thus, it plays a major role in semiconductor fabrication, where dopants are either introduced during a growing process or implanted, i.e., accelerated with high energy towards the SiC surface, where the dopant atoms kick out intrinsic atoms from their lattice location or reside on interstitial positions. The in-diffusion of dopants during growth processes produces less defects, but its application is limited by the the dopant diffusion which is very low in SiC. Implantation, on the other hand, can be performed up to saturation concentrations of dopants; however, the impacting ions cause heavy damage to the SiC crystal structure which must be repaired in a subsequent high-temperature annealing stage.

The implantation of 4H-SiC with varying Al ion doses has been described in our previous publication [1], where we also discussed the influence of the implantation temperature on the formation of intrinsic defects and the degree of amorphization in 4H-SiC.

To provide a large number of carriers in the band gap, the Al dopants must occupy Si-lattice sites in a nearly defect-free 4H-SiC crystal. To reduce the number of defects and to fully recrystallize the as-implanted SiC, thermal annealing is performed at temperatures of more than 1000 K [2]–[4].

High annealing temperature can help to re-establish order in the crystal by promoting the diffusion of defects; on the other hand, however, it also supports the agglomeration of interstitials into large amorphous clusters, which need long times to anneal out. Thus, it is important to investigate the basic mechanisms of recystallization as well as the role of the Al dopant in this process with respect to the impact of temperature and time. Our results have been discussed in comparison to experiments whenever available.

II. Methods

LAMMPS [5] is used to carry out the simulations, while OVITO [6] is used for visualization. The Gao-Weber (GW) potential [7] gives good predictions for the formation and migration energies and stable configurations for the intrinsic defects in 4H-SiC, in agreement with density functional theory (DFT) calculations. Moreover, the activation energies of the spontaneous recovery of Frenkel pairs [8] are consistant with experiments. Therefore, GW is used in the current MD simulations, together with the Ziegler-Biersack-Littmark (ZBL) term which models the repulsive force between the atoms. For the interaction of Al with Si and C atoms, the Morse potential, proposed by Dandekar and Shin [9] has been reparametrized for our study [1], with the parameters given in Table I to achieve a better agreement for the formation and migration energies of Al defects in 4H-SiC with DFT [10], [11].

TABLE I
Refitted parameters for the Morse Potential using a pair interaction cut-off of 5 Å.

System	Parameters	Morse-Potential
Al-Si	D_0	0.4
	α	1.6
	r_0	2.8
Al-C	D_0	0.4
	α	1.4
	r_0	2.05

The calculated migration barriers with the new Morse potential are given in Table II. As can be seen in the table, the diffusion barriers are in good agreement with DFT data and experiments performed with Al implanted SiC [12], while the kick-in/kick-out barriers are lower. The DFT barriers have, however, been calculated for the -1 charge state. DFT barriers for the uncharged state are closer to the values used in MD. As a consequence, activation/deactivation of Al occurs more

frequently than what is observed in experiments. The focus in the current study is the recrystallization of Al-implanted SiC, which is mainly driven by intrinsic defect recombination and migrations, processes described with sufficient accuracy by the GW potential.

TABLE II
ENERGY BARRIERS (EV) FOR AL DIFFUSION AND ACTIVATION IN 4H-SIC CALCULATED USING GAO-WEBER IN WITH AN OPTIMIZED MORSE POTENTIAL AND COMPARED TO PUBLISHED DFT DATA [10]

Barrier	Gao-Weber-Morse	DFT
Diffusion cubic plane	2.16	2.4
Diffusion hex plane	3.38	2.6
$Al_{hex} \rightarrow Al_{Si}+Si_{TC}$ (kick-in)	2.3	4.5
$Al_{hex} \leftarrow Al_{Si}+Si_{TC}$ (kick-out)	1.4	4.4

III. RESULTS AND DISCUSSION

The system implanted at room temperature and Al ion dose of 7.5×10^{14}/cm² has been chosen from [1] for the annealing study, as it shows the highest degree of amorphization. After implantation, the SiC structure was first equilibrated in the NPT ensemble at room temperature and zero pressure to relax compressive stresses built up during amorphization. The system was then heated up at rates of 10 K/ps to reach the final annealing temperatures ranging from 1000 K to 2500 K, followed by an annealing cycle for 100 ns.

In Fig. 1a, defect profiles for various annealing temperatures in comparison to the as-implanted profile are shown along the [0001] direction. The amorphous fraction gives the portion of amorphous atoms with respect to the total number of atoms in the same volume element, where the volume along the [0001]-axis was partitioned into 5 Å slices. The amorphous atoms, which also comprise interstitials, have been identified by the identify diamond structure (IDS) algorithm of OVITO. In Fig. 1b the maximum amorphous fractions centered around the profile peak are drawn over the annealing temperature. Although the annealing times between simulation (ns) and experiment (min) differ by many orders of magnitude, the general physical behavior of the system is maintained in the simulation. For instance, it was observed in experiments that full crystallization is initiated at a temperature of about 1300 K [2]–[4], with a residual defect fraction of around 10 %, which remains even at temperatures of up to 2000 K. Experimentally, it has also been shown that after annealing at lower temperatures, the structure does not recover its fully crystalline structure, even after many hours of annealing. The decrease in amorphous atoms during relaxation mostly comes from the recombination of Frenkel pairs, starting with activation energies of 0.2 eV [11].

The first annealing stage encountered during crystallization proceeds quickly, cf. Fig. 2, which is also in agreement with experiments [2]–[4], [13] and MD simulations [14] using the GW potential to study the recrystallization of a melt-quenched 4H-SiC. The activation energy for the recrystallization is displayed in the Arrhenius plot in Fig. 2b. The energy of 1.45 eV is somewhat lower than in the previous MD simulations [14]

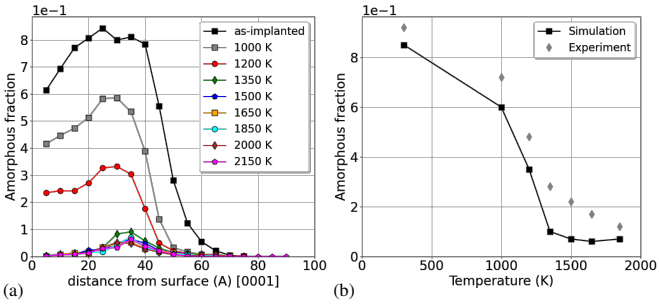

Fig. 1. (a) Profiles of IDS defect fractions along the [0001] direction deduced from OVITO [6] directly after implantation and after annealing for 100 ns at 1000 K to 2150 K. (b) Maximum amorphous fraction in ion implanted 4H-SiC in dependence of annealing temperature in comparison to experiment [4].

which calculated activation energies for the recyrstallization of up to 1.7 eV; however, this was for an amorphous system with a much larger number of homonuclear bonds/disorder. Experiments show activation energies from 1.3 eV to 3.4 eV [2], [3] for the structural recovery of different SiC polytypes, amorphized by ion implantation.

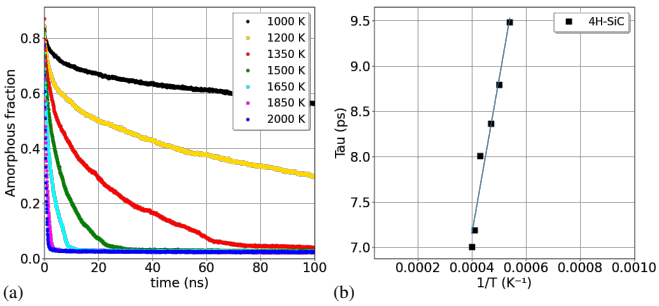

Fig. 2. a) Change of the amorphous fraction over time in dependence of the annealing temperature. b) Arrhenius plot for the crystallization time, giving an activation energy of 1.45 eV and a microscopic relaxation time τ_0 = 1.4 ps.

To further investigate this topic, we looked at the SiC structures at different times during annealing in Fig. 3. Cross sections through the areas of highest defect fraction were taken along the three main crystallographic axes in 4H-SiC. The annealing temperature was set to 1500 K (as the final amorphous fraction is smallest there) with snapshots displayed after 1 ns, 10 ns, 20 ns, and 100 ns of annealing, respectively. Amorphous atoms are shown in gray, the hexagonal layers in orange and green, while the cubic layers are marked in blue and cyan. Moreover, under-coordinated atoms indicating sp^2 atoms, vacancies, or dangling bonds are shown in red.

The recystallization proceeds from the amorphous/crystalline interface and is driven by epitaxial regrowth. Microscopically, this is a combination of local rearrangements of interstitials around defects, accompanied by diffusion processes. This explains the activation energy of around 1.5 eV, since migration barriers for the GW potential of Si and C are 1.5 eV and 0.7 eV, respectively [15], while Frenkel pair recombination takes place at energies between

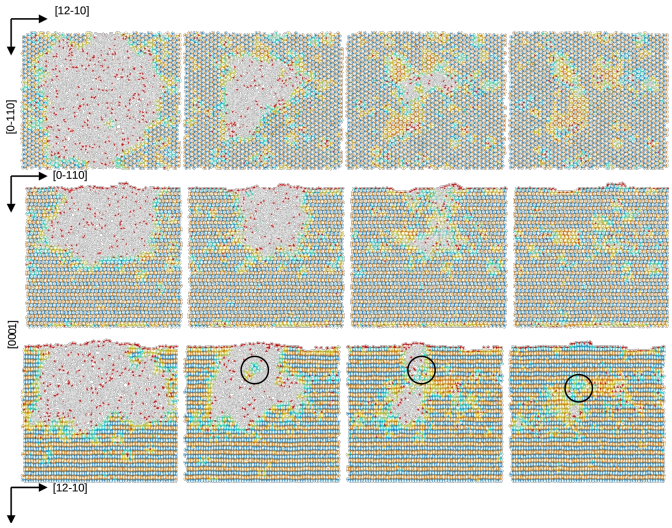

Fig. 3. Recrystallization along different crystallographic orientations (top to bottom) with snapshots taken at 1 ns, 10 ns, 20 ns, and 100 ns (left to right). The gray atoms indicate IDS atoms, cubic and hexagonal layers are depicted in blue and orange, under-coordinated atoms in red, respectively. The circles in the lower panel mark a spontaneously formed seed of a grain.

0.2 eV and 1.6 eV. During crystallization, about 40 % of the implanted Al ions were accommodated into the SiC lattice.

After around 30 ns the recrystallization is completed, and the SiC structure has become poly-crystalline. In the subsequent slower recovery regime, local kick-in/kick-out processes of the excess interstitials involving Al dominate, which have activation energies between 1.5 eV and 2.5 eV in the GW potential [1].

The final structure after annealing for 100 ns is comprised of 2H-SiC columns immersed in the direction of the surrounding 4H-SiC crystal. They originate from stacking faults created during relaxation of the SiC lattice. There are no grains of different orientations and poly-types formed, even when using higher annealing temperatures, as observed in MD simulations of [14] at 2000 K. Grains result from spontaneous nucleation growth, where it needs an amorphous cluster that is large enough to produce a stable grain. Only a small nucleus can be seen in the second image of the last row in Fig. 3 (circled) which produces a very small cubic domain at the end of the annealing cycle.

Grain formation needs longer annealing times than pure epitaxial regrowth. There are also strong variations in the experimentally achieved annealing times in dependence of grain size and polytype which range from a few seconds to many hours. The recrystallization time dependence on the grain size (existence) could be one possible explanation for the much faster relaxation times observed in MD simulations (nm sized) compared to experiments (μm sized). Al plays an additional role in the SiC recrystallization as it occupies native lattice sites on one hand and on the other hand provides dangling bonds to promote epitaxial regrowth. Thus, there are speculations [13] that implanted SiC recrystallizes faster than liquid-quenched SiC.

Beside larger defects like stacking faults and interstitial dislocation loops, the final annealed SiC structure contains smaller pure interstitial- and vacancy-clusters as well as bigger interstitial-vacancy clusters together with single point defects and defect pairs (complexes), circled in Fig. 4. As can be seen in the figure, which is also in agreement with experimental observations, interstitials preferentially agglomerate at stacking faults and around amorphous pockets. Interestingly, Al also substitutes for C lattice sites. It still needs to be investigated whether this is an artifact of the Morse potential or a physical effect.

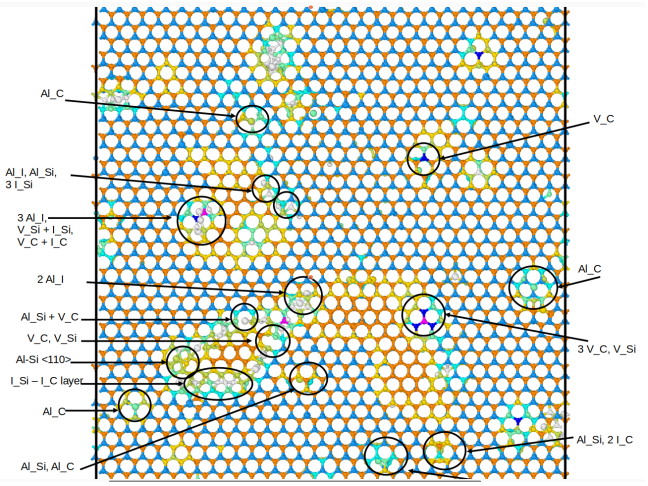

Fig. 4. Single defects and defect complexes marked by circles at the end of the annealing shown as an example at 1500 K on the 0001 surface by a cross section of the crystal at highest damage. Cubic atoms are in blue-cyan, hexagonal ones in orange-green, interstitials in grey. The notation is as follows: I_C, I_{Si} carbon and silicon interstitials, V_C (dark blue), V_{Si} (magenta), carbon and silicon vacancies, Al_I, Al_{Si}, Al_C (enlarged spheres) aluminum interstitials and Al occupying a silicon or carbon site, respectively.

There are many thermally stable intrinsic defects and defect-complexes [16] remaining after annealing, such as the carbon vacancy (V_C) related $Z_{1/2}$, $E_{H6/7}$ centers, the E_{H4} center which is a carbon antisite - vacancy complex (C_{Si}-V_C) or the di-vacancy (V_{Si}-V_C). All vacancy related defects are known for their high annealing activation energies of more than 4 eV, required for vacancy migration. Moreover, carbon interstitial-(I_C-I_C), carbon interstitial - antisite- (I_C-C_{Si}) and carbon - silicon interstitial (I_{Si}-I_C) clusters with binding energies between 2 eV and 10 eV [17]–[19] - depending on cluster size - are formed. Al also forms very stable thermally immobile complexes [10], [20] like the DLTS center, consisting of Al-V_C with a binding energy of 0.6 eV, or small interstitial clusters consisting of Al_I-I_{Si}-I_C with binding energies ranging from 1.7 eV to 5.8 eV.

In Fig 5 the concentration of selected point defects and Al related complexes after recrystallization at different temperatures are shown. While complexes like the Al-C, V_C-V_{Si} and C_{Si}-VC are nearly independent of the annealing temperature, considerably less interstitials and vacancies remain after high temperature annealing, since the moving interstitials recom-

bine with vacancies. Moreover, the number of Al atoms on lattice sites increases with temperature.

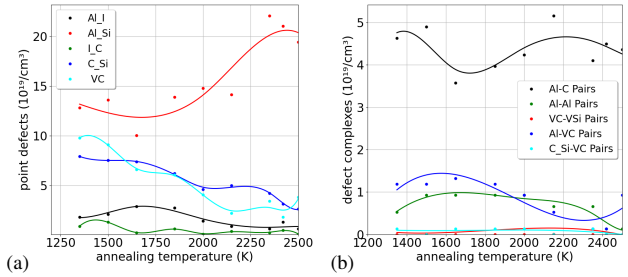

Fig. 5. (a) The concentration of various selected point defects in dependence of the annealing temperature and (b) the concentration of Al related complexes and the di-vacancy in dependence of the annealing temperature.

Different annealing temperatures lead to different final crystal structures. While for annealing temperatures of up to 2000 K extended defects are mainly represented by stacking faults, higher temperatures promote the formation of large amorphous clusters in an otherwise more or less mono-crystalline substrate. This behavior is depicted in Fig. 6, where maximum cluster sizes of several hundred defects can be reached with annealing temperatures of 2500 K. Those clusters are created by the residual interstitials which are more mobile and able to diffuse longer distances at high temperatures. The clusters act like sinks for the interstitials and need long times to dissolve during annealing (longer than accessible in conventional MD).

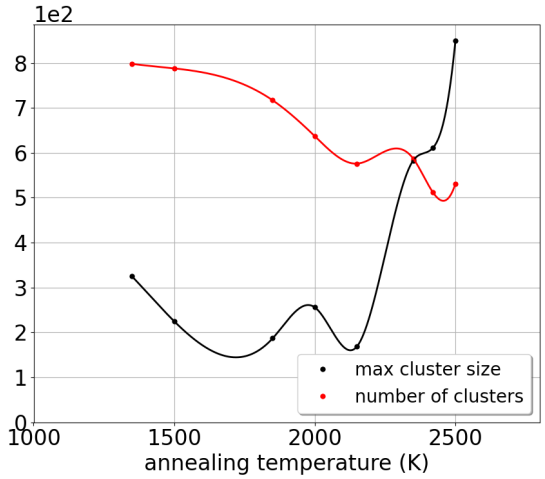

Fig. 6. Maximum cluster sizes and number of clusters in dependence of the annealing temperature

A detailed statistical analysis is necessary to find a correlation between the number of remaining stable defects and the annealing temperature. Moreover, also implantation temperature and Al dose have a decisive impact on the final SiC defect structure.

IV. Conclusion

We have performed an MD annealing study of Al implanted 4H-SiC, showing that the temperature of 1300 K at which SiC fully recrystallizes could be reproduced with MD. Moreover, a residual defect fraction of 10 % for annealing temperatures of more than 2000 K is in line with experiments. The recrystallization is driven by epitaxial regrowth. The lack of grain formation could be one reason for the faster recrystallization at high temperatures and the slightly lower activation energy compared to experiments [2]. The annealed structure shows many defects such as stacking faults, amorphous clusters, defect complexes, and single point defects in dependence of temperature. Most of these defects are extremely long-lasting and need high temperatures and long relaxation times to anneal out.

A statistical evaluation is ongoing to find the correlation between annealing temperature, implantation temperature, ion dose, and the number and type of defects in the annealed SiC structure and the defect formation/annihilation. Moreover, an improved SiC-Al potential is currently developed using a machine learning approach to have a better description of the Al activation.

Acknowledgement

Financial support by the Federal Ministry of Labour and Economy, the National Foundation for Research, Technology and Development and the Christian Doppler Research Association is gratefully acknowledged.

References

[1] S. Leroch *et al.*, *Proc. SISPAD*, Kobe, Japan, 2023.
[2] A. Höfgen *et al.*, *Mat. Sc. and Eng. B*, **61**, 353, 1999.
[3] E. Wendler *et-al.*, *Nuc. Instr. and Methods in Phys. Res. B* **141**, 105, 1998.
[4] S. Miro *et al.*, *Phil. Mag.* **94**, 3898, 2014.
[5] A.-P. Thompson *et al.*, *Comp. Phys. Comm.* **27**, 108171, 2022.
[6] A. Stukowski, *Model. Simul. Mater. Sci. Eng.*, **18**, 015012, 2009.
[7] F. Gao and W. J. Weber, *Nucl. Instrum. Methods Phys. Res. B* **191**, 504, 2002.
[8] F. Gao *et al.*, *J. Appl. Phys.* **94**, 4348, 2003.
[9] C. R. Dandekar and Y. C. Shin, *Compos. Part A Appl.* **42**, 355, 2011.
[10] Y. Huang *et al.*, *J. Appl. Phys.* **132**, 015701, 2022.
[11] A. Mattausch, *PhD. Thesis, Universität Erlangen Nürnberg*, 2005.
[12] Y. Tajima *et al.*, *J. Chem. Phys.*, **77**, 2582, 1982.
[13] M. Satho *et al.*, *Nuc. Instr. and Methods. in Phys. Res. B*, **242**, 627, 2006.
[14] F. Gao *et al.*, *Phys. Rev. B* **74**, 104108, 2006.
[15] F. Gao *et al.*, *Phys. Rev. B* **69**, 245205, 2004.
[16] J. Coutinho, *Crystals* **11**, 167, 2021.
[17] A. Mattausch *et al.*, *Phys. Rev. B* **70**, 235211, 2004.
[18] T. Hornos, *PhD. Thesis, Universität Budapest*, 2008.
[19] C. Jiang *et al.*, *Phys. Rev. B* **86**, 144118, 2012.
[20] A. Gali *et al.*, *Phys. Rev. B*, **75**, 045211, 2007.